JGR Atmospheres

RESEARCH ARTICLE
10.1029/2020JD034353

Special Section:
The Exceptional Arctic Polar Vortex in 2019/2020: Causes and Consequences

Vertical Structure of the Arctic Spring Transition in the Middle Atmosphere

Vivien Matthias[1], Gunter Stober[2], Alexander Kozlovsky[3], Mark Lester[4], Evgenia Belova[5], and Johan Kero[5]

[1]Deutsches Zentrum für Luft- und Raumfahrt, Institut fr Solar-Terrestrische Physik, Neustrelitz, Germany, [2]Institute of Applied Physics & Oeschger Center for Climate Change Research, Microwave Physics, University of Bern, Bern, Switzerland, [3]Sodankylä Geophysical Observatory of the University of Oulu, Sodankylä, Finland, [4]University of Leicester, Leicester, UK, [5]Swedish Institute of Space Physics, Kiruna, Sweden

Abstract In the middle atmosphere, spring transition is the time period where the zonal circulation reverses from winter westerly to summer easterly which has a strong impact on the vertical wave propagation influencing the ionospheric variability. The spring transition can be rapid in form of a final sudden stratospheric warming (SSW, mainly dynamically driven) or slow (mainly radiatively driven) but also intermediate stages can occur. In most studies spring transitions are classified either by their timing of occurrence or by their vertical structure. However, all these studies focus exclusively on the stratosphere and it is not clear if and how pre-winter conditions have an impact on when and how spring transitions take place. Here we classify the spring transitions regarding their vertical-temporal development beginning in January and spanning the whole middle atmosphere in the core region of the polar vortex. This leads to five classes where the timing of the SSW in the preceding winter and a downward propagating Northern Annular Mode plays a crucial role. First, we use Microwave Limb Sounder satellite data to describe the five classes for recent single years, and then we use Modern-Era Retrospective analysis for Research and Applications Version 2 reanalysis data for a composite analysis. The results show distinctive differences between the five classes in the months before the spring transition especially in the mesosphere. We hypothesize that this will help to improve the prediction of the spring transition. Additionally, meteor radar winds are used to link spring transition effects in the upper mesosphere and lower thermosphere with the stratospheric final warming.

Plain Language Summary Springtime is characterized by a dramatic change in circulation from winter westerly to summer easterly in the Arctic middle atmosphere (20–100 km). The timing and structure of this change process largely varies from year to year. In most studies spring transitions are classified either by their timing of occurrence or, slightly less common, by their vertical structure. However, all these studies focus on the stratosphere (20–50 km) only and do not consider a large part of the spring transitions because they only investigating for example, particularly early or late occurring spring transitions. Here we classify the spring transitions regarding their vertical and temporal development already starting in mid-winter. This leads to five classes where the timing of large polar vortex disturbances in the preceding winter as well as the vertical structure of the polar vortex plays a crucial role. This allows a certain prediction at least for some of the five spring transition classes. Additionally, the spring transition in the upper mesosphere and lower thermosphere (80–100 km) is investigated regarding the new spring transition classes and its impact on the ionosphere and therefore on our communication and navigation system is discussed.

Key Points:

- There are five new classes of spring transitions in the middle atmosphere
- The classification uses the temporal-vertical structure of zonal wind and Northern Annular Mode starting in January
- The classification enables a better understanding of the timing and type of the spring transition

Supporting Information:

Supporting Information may be found in the online version of this article.

Correspondence to

V. Matthias,
vivien.matthias@dlr.de

Citation:

Matthias, V., Stober, G., Kozlovsky, A., Lester, M., Belova, E., & Kero, J. (2021). Vertical structure of the Arctic spring transition in the middle atmosphere. *Journal of Geophysical Research: Atmospheres*, *126*, e2020JD034353. https://doi.org/10.1029/2020JD034353

Received 2 DEC 2020
Accepted 19 APR 2021

Author Contributions:

Conceptualization: Vivien Matthias
Data curation: Gunter Stober, Alexander Kozlovsky, Mark Lester, Evgenia Belova, Johan Kero
Formal analysis: Vivien Matthias
Investigation: Vivien Matthias
Software: Gunter Stober
Writing – original draft: Vivien Matthias

1. Introduction

In the middle atmosphere (10–100 km) spring is the time period when the winter westerly winds reverse to summer easterly winds. The final breakdown and warming of the polar vortex is in general called "stratospheric final warming" (SFW). The timing and dynamical evolution of the stratospheric final warming is characterized by a combination of radiative forcing, due to seasonal changes of the solar zenith angle, and planetary wave (PW) forcing effects due to nonlinear interactions of PWs with the mean flow (Butler et al., 2019; Salby & Callaghan, 2007; Waugh et al., 1999). These dynamical processes significantly influence

not only the date of the springtime polar vortex breakup but also its vertical development and the speed of transition from westerly to easterly winds (Hardiman et al., 2011; Hu, Ren, Yu, & Xu, 2014; Wei, 2007).

In the northern hemisphere there is a large interannual variability in the onset dates of the SFW varying by about 2 months between early March and late May (Butler et al., 2019; Savenkova et al., 2012; Wang et al., 2019; Waugh et al., 1999). The temporal-vertical structure of the zonal wind reversal also varies from year to year where the wind reversal can first occur in the upper or middle stratosphere or even simultaneously at all altitudes in the stratosphere (Hardiman et al., 2011; Thiélemont et al., 2019). Additionally, the wind reversal can be sudden, indicative of stronger wave forcing, or gradual, indicative of radiative relaxation as the dominant process (Butler et al., 2019).

All studies investigating the spring transition in the stratosphere use a classification of the stratospheric final warming. The most common way is to distinguish SFWs by the timing of their onset in the middle stratosphere into early and late SFWs (Akiyoshi & Zhou, 2007; Ayarzagüena & Serrano, 2009; Butler et al., 2019; Kelleher et al., 2020; Li et al., 2012; Waugh & Rong, 2002; Wei, 2007). A second way is to classify SFWs by their vertical-temporal development in the stratosphere rather than by their timing. Here, the SFWs are distinguished by the first occurrence of the wind reversal at 10 or 1 hPa (Hardiman et al., 2011; Thiélemont et al., 2019). Other classification methods, but less common, are by distinguishing between synchronous and asynchronous SFWs (Wang et al., 2019) or by the occurrence of Sudden Stratospheric Warmings (SSWs) in the preceding winter (Hu et al., 2015).

There are two main modes to distinguish between early and late SFWs, one is based on the potential vorticity (Nash et al., 1996; Waugh et al., 1999) and the other one on zonal winds (e.g., Black & McDaniel, 2007; Labitzke, 2000). The most common approach is using the zonal wind since the zonal wind in the stratosphere influences the upward propagation of waves and hence the coupling between the different atmospheric layers (Wei, 2007). Using the zonal wind, the SFW date is defined as the day when the zonal mean zonal wind in the core region of the polar vortex (10–50 hPa, 60–70°N) drops below zero without returning to a specified threshold value until subsequent fall. The mean climatological SFW date is between fourth and 17th April depending on the data set (Black et al., 2006; Butler et al., 2019; Wei, 2007). Early and late SFWs are then defined by exceeding ± 1.0 standard deviations from the average respectively (Ayarzagüena & Serrano, 2009; Kelleher et al., 2020; Li et al., 2012; Wei, 2007). Early SFWs occur on average in the second half of March while late final warmings occur on average in the first half of May (Li et al., 2012). In early SFW years the wind reversal to easterly winds happens on average rather quickly within a few days, starts at upper stratospheric levels and propagates downward to lower levels (Ayarzagüena & Serrano, 2009; Li et al., 2012; Wei, 2007). There are strong easterly winds in the middle stratosphere directly after the SFW, which weaken in the following weeks, but never get westerly until subsequent fall (Butler et al., 2019; Hu, Ren, Yu, & Xu, 2014; Li et al., 2012; Wei, 2007). However, after some early SFWs, a reconstruction of westerly winds can be observed in the upper stratosphere (Ayarzagüena & Serrano, 2009; Wei, 2007). In late SFW years the westerly wind decreases on average gradually and almost simultaneously at all levels (Hu, Ren, Yu, & Xu, 2014; Wei, 2007). While early SFWs are characterized by a strong wave activity before the wind reversal, which decreases sharply afterward, only a weak wave activity is observed around late SFWs (Hu, Ren, & Xu, 2014; Wei, 2007). Thus, early SFWs are mainly dynamically driven, while late SFWs are mainly radiatively driven.

The classification between 10 hPa-first and 1 hPa-first SFWs works similar to the early and late classification. Here, the day when the wind reverses to easterly in the core region of the polar vortex is calculated for every vertical level resulting in a vertical-temporal information about the final wind reversal (Hardiman et al., 2011; Thiélemont et al., 2019). The key difference is whether or not the SFW takes place first in the middle stratosphere. SFWs occurring first in the middle stratosphere and later in the upper stratosphere imply that the upper stratosphere is then somewhat decoupled from the middle and lower stratosphere since waves are unable to propagate through the mean easterly flow at 10 hPa and hence the upper stratospheric final warming is expected to be dominated by radiative processes (Hardiman et al., 2011). Stratospheric final warmings classified as 1 hPa-first start in the mesosphere and propagate downward through the stratosphere with time. On average, 10 hPa-first SFWs occur around 10 April, while 1 hPa-first final warmings occur around 20 April at 1 hPa and later at 10 hPa (Thiélemont et al., 2019). Thus, in general, 1 hPa-first events occur later than 10 hPa-first events. Shortly before 10 hPa-first events planetary waves break at 10 hPa and

thus decrease the zonal wind below, while for 1 hPa-first events the PWs break around 1 hPa (Hardiman et al., 2011; Thiélemont et al., 2019).

There is a huge interest in predicting the timing and vertical structure of SFWs due to its potential role in tropospheric and ionospheric predictions also on subseasonal to seasonal time scales (Butler et al., 2019; Yiğit & Medvedev, 2015). Several studies found a linkage between the timing of SFWs and the polar vortex conditions in the preceding winter (e.g., Hu et al., 2015; Newman et al., 2001; Waugh et al., 1999; Wei, 2007). The occurrence of SSWs in previous winter affects both the timing and type of SFWs in the following spring (Hu, Ren, & Xu, 2014; Thiélemont et al., 2019). While early SFWs are mostly preceded by non-SSW winter, late SFWs are mostly preceded by major SSW winter (Hu, Ren, & Xu, 2014). More generally, SFWs will be delayed when major or minor SSW events occur in the preceding winter (Hu et al., 2015). However, the occurrence or absence of SSWs in the previous winter is not sufficient to anticipate a late or early SFW in the following spring (Hu et al., 2015; Hu, Ren, & Xu, 2014). More recently, Thiélemont et al. (2019) found that winters with a SSW are more likely followed by a 10 hPa-first SFW, while winters without SSWs usually end up with 1 hPa-first final warmings. Additionally, SSWs occurring in winter preceding a 1 hPa-first event are earlier in the season than SSWs preceding a 10 hPa-first SFW event in spring (Thiélemont et al., 2019).

SSWs are accompanied by a negative Northern Annular Mode (NAM) index which can propagate downward into the troposphere influencing our weather for up to eight weeks (Baldwin & Dunkerton, 2001). In the middle atmosphere the NAM index is a manifestation of the strength of the polar vortex where large positive values stand for a strong polar vortex, while negative values represent a breakdown of the polar vortex. Thus, the NAM variability is largely driven by wave forcing. The downward propagating negative NAM during SSWs is associated with a suppression of PW activity in the stratosphere which might explain the general weakness of PW activity and late SFWs after mid-winter SSWs (Hu, Ren, & Xu, 2014). Savenkova et al. (2012) even found a link between the NAM index in the middle stratosphere and the SFW date, describing that the lower the NAM index in mid stratosphere in March and April, the earlier the final warming. However, March and April are the months where the early SFWs take place making it difficult to interpret the results especially considering the results of Li et al. (2012). They found a positive NAM signal before and a negative NAM signal after both early and late SFWs in the mid and upper stratosphere. These signals are stronger for early SFWs and propagate downward into the troposphere. Thus, the negative NAM signals in the regression analysis of Savenkova et al. (2012) might originate from the SFW itself. Nevertheless, it seems that there is a connection between the SFW and the behavior of the NAM index.

Studies investigating the spring transition in the northern hemisphere mesosphere and ionosphere are much rarer and less systematic than stratospheric studies. Hoffmann et al. (2010) investigated the zonal wind reversal in spring 2008 in the mesosphere and lower thermosphere (MLT) which was characterized by an abrupt transition to easterly winds at all heights (70–100 km) simultaneously. At 91 km the average wind reversal occurs at 24th March with a standard deviation of 9 days whereas the year-to-year variability of MLT zonal wind reversal correlates with stratospheric polar vortex variability (Aushev et al., 2006; Merzlyakov et al., 2012). Closely related to the wind reversal in the MLT in spring is an enhancement followed subsequently by a strong decrease in atomic oxygen and temperature (G. G. Shepherd et al., 1999; M. G. Shepherd et al., 2002). Additionally, during some spring transitions, oscillations of 10–16 days are observable in the MLT and ionosphere (Gordienko et al., 2007; Yamazaki & Matthias, 2019; Yu et al., 2019) generated by instabilities in the stratosphere and lower mesosphere (Yamazaki & Matthias, 2019).

All studies mentioned above either investigate the spring transition systematically in the stratosphere only, or they investigate the spring transition in the MLT region only, decoupled from the stratospheric studies and without being systematic. Thus, systematic studies of the spring transition covering the whole middle atmosphere are missing. Furthermore, the classification of SFWs, which has been used so far, leads to a systematic neglect of many SFWs, since all SFWs, which are neither early nor late or happen simultaneously at all altitudes, are not considered at all. Additionally, while it is generally accepted that the occurrence or absence of SSWs in the preceding winter has an impact on the SFW, only tendencies can be given for the timing and type of SFWs in the following spring. Therefore, it is still not possible to predict the timing and type of the final wind reversal during the northern hemisphere spring transition.

Here, we want to introduce a new type of classification according to the vertical-temporal evolution of the zonal mean zonal wind in the core region of the polar vortex *and* the NAM index between January and May in the stratosphere *and* mesosphere. This way, we systematically investigate the spring transition in the *whole middle atmosphere* and include *all* spring transitions between 1980 and 2020. Additionally, this new spring transition classification already includes the timing and type of SSWs in the preceding winter, making a prediction of the timing and type of the final wind reversal for some of the new classes probably more feasible. Note, that we will call the final zonal wind reversal covering all altitudes in the middle atmosphere *spring transition* in the following, to not confuse with the SFWs which focuses on the stratosphere only.

The study is structured as follows: Section 2 describes the data and methods. Section 3 first introduces the new classification using single years and global satellite observations from Aura Microwave Limb Sounder (MLS) and then examines their mean characteristic using global reanalysis data from Modern-Era Retrospective analysis for Research and Applications Version 2 (MERRA-2). The results are then compared to local mesospheric radar observations and discussed in Section 4. A summary and conclusion of the study is provided in Section 5.

2. Data and Methods

Investigating the spring transition in the Arctic middle atmosphere requires data sets spanning the polar cap northward of 50°N. Therefore, we use global satellite observations from MLS and reanalysis data from MERRA-2. We also combine these with local radar measurements to cover the MLT region where the vertical resolution of MLS is not sufficient and MERRA-2 gives no data at all.

2.1. MLS Satellite Data

To show exemplarily the newly introduced classes of spring transitions from the lower stratosphere to the upper mesosphere, we use global geopotential height (GPH) data from the MLS on board the Aura satellite (Livesey et al., 2015; Waters et al., 2006). MLS has a global coverage from 82°S to 82°N on each orbit, and a usable height range from approximately 11 to 97 km (261–0.001 hPa) with a vertical resolution of ∼4 km in the stratosphere and ∼14 km at the mesopause. The temporal resolution is 1 day at each location, and data are available since August 2004 until today (Livesey et al., 2015). Version 4 MLS data were used and the most recent recommended quality screening procedures of Livesey et al. (2015) have been applied.

For our analyses the original orbital MLS data are accumulated in grid boxes with 10° grid spacing in longitude and 5° in latitude. Afterward, they are averaged at every grid box and for every day, generally resulting in a global grid with values at every grid point. The geostrophic neutral zonal wind is then calculated as described in Matthias and Ern (2018).

2.2. MERRA-2 Reanalysis Data

Average characteristics of the different classes are then investigated using global reanalysis data from the MERRA-2 (Bosilovich et al., 2015; Gelaro et al., 2017; Molod et al., 2015). Here we use daily means of the 3-hourly instantaneous output on 42 constant pressure levels ranging from 1,000 to 0.1 hPa, that is, from the surface up to approximately 64 km. The horizontal resolution is 0.625° in longitude and 0.5° in latitude. For our analysis we use MERRA-2 reanalysis neutral wind data from winter 1980 to 2020, that is, 41 spring transitions in total. Note that MERRA-2 assimilates temperature and ozone profiles from MLS satellite in the upper stratosphere and mesosphere starting in August 2004 (Gelaro et al., 2017).

2.3. Meteor Radar Winds Above Nordic Countries

Since the vertical resolution of MLS is low (∼14 km) in the MLT, we complement the global observations of MLS with local radar measurements by a merged data set from Esrange (68°N, 21°E) near Kiruna in Sweden and Sodankylä (67°N, 26° E) in Finland to discuss the impact of the newly defined spring transition classes on the MLT region in polar regions. The Esrange meteor radar is a SKiYMET (All-Sky Interferometric Meteor Radar) radar which is described in more detail by Mitchell et al. (2002) and details of the Sodankylä

meteor radar are presented in Lukianova et al. (2015); Lukianova et al. (2018). Background MLT neutral winds, where solar tides are subtracted, are obtained with a temporal resolution of 1 h and a vertical resolution of 2 km using the wind retrieval algorithm as described in Stober et al. (2020) and Baumgarten and Stober (2019), which is a further development of the wind analysis of Hocking et al. (2001). The merged data set contains continuous wind data since August 1999 resulting in 21 spring transitions and thus, it is now the longest available continuous wind meteor radar observation on the globe. For the composite analysis of MLT winds, daily mean values of the background winds are used that were smoothed by a 15-day running mean, similar to Merzlyakov et al. (2012) due to the high variability of this region.

2.4. Methods

There are a lot of different definitions for the SFW onset day using the zonal wind (e.g., Butler et al., 2019; Hu, Ren, Yu, & Xu, 2014; Wei, 2007). They all have in common that they use the zonal mean zonal wind reversal somewhere in the core region of the stratospheric polar vortex. Here, we follow in general these definitions and use the reversal of zonal mean zonal wind averaged between 60° and 70°N but apply it to all pressure levels in the middle atmosphere resulting in different dates for different pressure levels. To investigate the latitudinal and vertical structure of the spring transition in the middle atmosphere, we also apply this definition to all latitudes northward of 50°N.

Because of the close relation between NAM and SSW, we additionally use the information on the duration and strength of the downward propagating NAM index to classify the spring transition. As a simple proxy for the NAM index we follow Karpechko et al. (2017) and calculate the normalized anomaly of the geopotential height averaged over the polar cap (60°−90°N), which is tightly linked to the NAM index defined by the empirical orthogonal function (Baldwin & Thompson, 2009). Anomalies of the polar cap geopotential height are calculated with respect to the annual climatology for each calendar day at all pressure levels and then normalized by their standard deviations. The phase of the NAM is conventionally defined to be negative when polar cap geopotential height anomalies are positive, thus, we multiply our polar cap geopotential height anomalies by minus 1.

To investigate average characteristics of the newly defined spring transition classes, composite analyses are applied mostly with the reference day first of January but also centered around the day when the zonal mean zonal wind finally reverses at a certain altitude. We base our statistical analysis on the null hypothesis that the spring transition class test statistic is exactly the same as the population value from which it is drawn. We apply a bootstrap method with replacements (Grotjahn & Faure, 2008) to determine the significance of the composites of the different spring transition classes at each day and altitude. For that, the number of randomly selected years for the bootstrap is kept equal to the observed years in the corresponding spring transition class. A detailed description of the statistical considerations and the bootstrap algorithm can be found in Grotjahn and Faure (2008).

3. Results and Discussion

In the following we will first introduce the new spring transition classification by describing the different classification features of the different classes based on selected years using MLS satellite data. Afterwards, average characteristics of the different classes are investigated using MERRA-2 data.

3.1. Introduction of the New Spring Transition Classes

Commonly, stratospheric final warmings are classified using the zonal mean zonal wind in the core region of the polar vortex, that is, the area of maximum wind values (e.g., Butler et al., 2019; Li et al., 2012; Wei, 2007). Here, we follow in general this notification by using the zonal mean zonal wind in the core region of the polar vortex but do not only use the onset of the wind reversal itself but the vertical-temporal evolution of the zonal mean zonal wind starting in January of the same year. This way, possibly occurring SSWs are already included in the classification. Note that we do not start in early winter because Thiélemont et al. (2019) and Hu, Ren, Yu, and Xu (2014) found that SSWs occurring in early winter do not have an impact on the stratospheric final warming type and date due to the relatively long time lapse before the spring

transition that allows the recovery of a strong polar vortex. Additionally, to the zonal wind, we also use the NAM index to classify spring transitions in the middle atmosphere. The NAM index is important since SSWs accompanied by a strong downward propagating negative NAM and lasting for several weeks, as described in Baldwin and Dunkerton (2001), have a different impact on the final wind reversal type and timing than SSWs without a downward propagating NAM, as will be shown below. Because we classify the spring transitions with respect to the occurrence of SSW, we apply the spring transition class names *"mid-winter SSW", "late-winter SSW", "early spring SSW", "mid-spring SSW"* and *"No negative NAM"*. These will be described in the following in detail.

As a start the different classes are exemplarily illustrated based on five selected springs. Figure 1 shows the temporal-vertical evolution of the zonal mean zonal wind averaged between 60° and 70°N (left) and the NAM index (right) from January to May for five different years. Shown are the spring transitions in 2013, 2018, 2016, 2015, and 2020. The sorting of the different years is not chronological but sorted by the timing of occurrence of a major SSWs partly resulting in a final wind reversal (see Figures 1a–1d).

In 2013, a major SSW occurs in January reversing the zonal wind from westerly to easterly in the whole middle atmosphere (see Figure 1a), accompanied by a strong negative downward propagating NAM lasting until March in the lower stratosphere (see Figure 1f). After the SSW, a strong polar vortex forms in the mesosphere with wind values above 100 ms^{-1} and downward propagating into the lower stratosphere over the next hundred days. At the same time a strong positive and also downward propagating NAM signal occurs after the SSW. The spring transition itself starts in the upper mesosphere and propagates downward with time and reaches the 10 hPa level at the beginning of May. The transition from winter westerly to summer easterly winds is smooth in all altitudes. Thus, the main features of this class are a major SSW in January accompanied by a strong negative downward propagating NAM and followed by the recovery of a strong polar vortex in the mesosphere. This results in a smooth and downward propagating spring transition, which occurs quite late. We call this class *"mid-winter SSW"*.

In 2018, a major SSW occurs in February and thus about 1 month later as in the first class, but again accompanied by a strong negative downward propagating NAM and a recovery of the polar vortex in the mesosphere although with a smaller magnitude compared to 2013 (see Figures 1b and 1g). Similar to 2013 the strong westerly winds propagate downward with time but, in contrast to 2013, never reach the lower stratosphere. In the lower and middle stratosphere the zonal wind remains weak and even reverses again for a certain time before the final wind reversal occurs in mid-April. However, the final wind reversal in the mesosphere again propagates downward with time, whereas the latest wind reversal occurs at the beginning of May around the stratopause region and thus much later than in the stratosphere. The main features of this class are a major SSW in late-winter accompanied by a negative downward propagating NAM and followed by a recovery of the polar vortex in the mesosphere. However, in this class, the temporal evolution of the spring transition differs in the stratosphere and the mesosphere. Similar to 2013 the mesospheric wind reversal propagates downward with time, while the stratospheric wind reversal occurs much earlier and simultaneously at all altitudes. We call this class *"late-winter SSW."*

In 2016, a minor SSW occurred in February but without the characteristical downward propagating negative NAM (see Figures 1c and 1h). However, beginning of March a major SSW occurs accompanied by the downward propagating negative NAM. This SSW leads to a final wind reversal to summerly easterly winds in the lower and middle stratosphere and in the upper mesosphere. However, between 40 and 80 km the winterly westerly winds recover for over a month resulting in winterly westerly winds in the upper stratosphere and mesosphere surrounded by summerly easterly winds. The latest wind reversal in the spring transition occurs at the end of April near the stratopause region and thus over one month later than in the middle stratosphere. The main features of this spring transition class are a major SSW in early spring accompanied by a negative downward propagating NAM resulting in a final springtime wind reversal below 40 km and above 80 km. In the area between 40 and 80 km winter conditions recover and the final wind reversal in that region takes place much later than in the lower and middle stratosphere. We call this class *"early spring SSW"*.

In 2015, a minor SSW occurs at the beginning of January but without the characteristical downward propagating negative NAM (see Figures 1d and 1i). However, at the beginning of April a major SSW occurs, accompanied by a downward propagating negative NAM. This SSW acts as a spring transition finally reversing

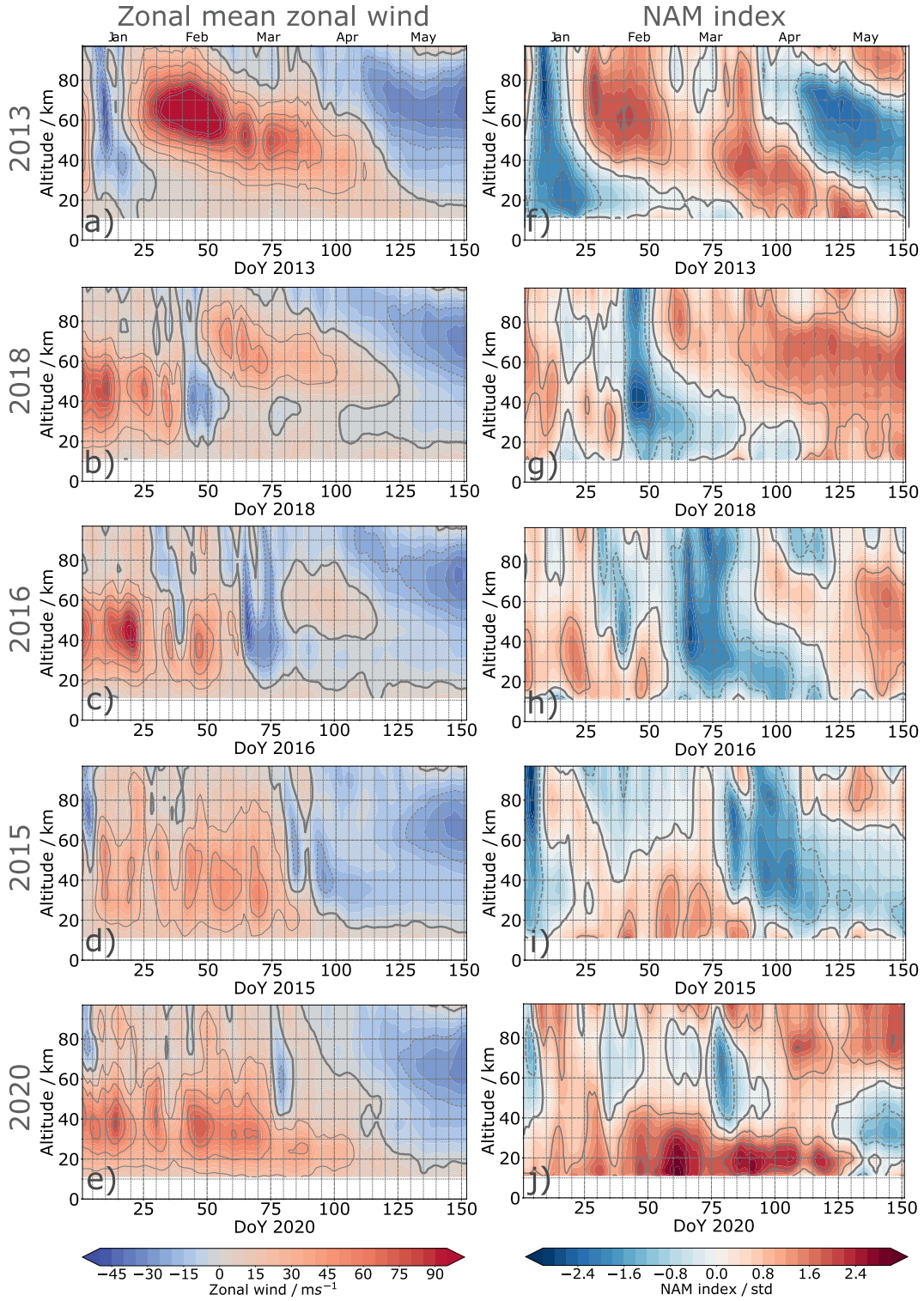

Figure 1. Left: Time-height cross-section of the zonal mean zonal geostrophic wind averaged between 60° and 70°N (left) and NAM index (right). Data are derived from MLS GPH observations in both cases and shown for spring transitions in 2013, 2018, 2016, 2015, and 2020. GPH geopotential height; MLS, Microwave Limb Sounder; NAM, Northern Annular Mode.

the wind at all altitudes almost simultaneously. Note, that this SSW is not a SSW in the traditional sense but is commonly classified as a final warming (Butler et al., 2017). The main features of this spring transition class are a major SSW in mid-spring accompanied by a negative downward propagating NAM and resulting in a final springtime wind reversal simultaneously at all altitudes. We call this class *"mid-spring SSW"*.

In 2020, a minor warming occurs in mid-March having the potential to finally reverse the zonal wind (see Figures 1e and 1j). However, this minor SSW is not characterized by a downward propagating negative NAM and thus the zonal winds become westerly again although the magnitude is weaker after the minor SSW than before. The final wind reversal during the spring transition starts in the upper mesosphere in mid-April and propagates downward with time, reaching the lower stratosphere beginning of May. Note, that this downward propagation is not such a smooth processes as it is in 2013. The main feature of this spring transition class are the absence of a negative downward propagating NAM and a smooth spring transition that propagates downward with time, occurring quite late. We call this class *"no negative NAM"*.

In the next section the average characteristics of these five spring transition classes are investigated more closely and possibilities for a prediction of the type and timing of the spring transition are discussed.

3.2. Average Occurrence of the Five Spring Transition Classes

To classify the 41 spring transitions included in the MERRA-2 data set, the spring transition characteristics described in Section 3.1 are now generalized and thresholds are given which are not strictly defined but give an orientation. Note, that to use this kind of classification to improve the prediction of spring transitions, more strictly defined thresholds are needed which are beyond the scope of this study. For the classification, the zonal mean zonal wind ($\overline{u}$) anomaly normalized by its standard deviation and the NAM index are used at 10 and 0.3 hPa. The average temporal development of these variables are shown for each spring transition class in Figure S1 in the supporting information.

Mid-winter SSW spring transitions are marked by an excess of $\overline{u}$ and NAM of −1.0 std at 10 hPa sometime in January to early February for several days to weeks describing the major SSW in January. Note, that $\overline{u}$ and NAM are also negative in January at 0.3 hPa but for a much shorter time period than at 10 hPa. Later in February and March, $\overline{u}$ and NAM exceed +1.0 std at 0.3 hPa for approximately 40 days after the $std(\overline{u})$ minimum at 10 hPa and again +1.0 std at 10 hPa in April characterizing the downward propagation of the strong westerly wind and NAM from the mesosphere into the stratosphere. Thus, after the major SSW in January the zonal mean zonal wind remains westerly in the whole middle atmosphere until the final wind reversal in May.

Late-winter SSW spring transitions are marked by an excess of $\overline{u}$ and NAM of −0.75 std at 10 hPa sometime between mid-February and mid-March for several days describing the major SSW. Note, that $\overline{u}$ and NAM are also negative in February at 0.3 hPa but again for a shorter time period than at 10 hPa. Similarly, but later and weaker compared to mid-winter SSW spring transitions, $\overline{u}$ and NAM exceed +0.5 std at 0.3 hPa between mid-March and mid-April for approximately 40 days after the $std(\overline{u})$ minimum at 10 hPa. In contrast to *mid-winter SSW* spring transitions, the zonal mean zonal wind is predominantly westerly but weak after the major SSW in February in the stratosphere and can be even easterly for several days before the final wind reversal occurs.

Early spring SSW spring transitions are marked by an excess of $\overline{u}$ and NAM of −0.75 std at 10 and 0.3 hPa in March describing the major SSW or respectively final warming. This SSW is associated with a final wind reversal to easterly winds in the stratosphere but **not** in the mesosphere. Thus, after the SSW, westerly winds are observed in the mesosphere for at least one week. Again, during the SSW the time period where $\overline{u}$ and NAM are negative is shorter in the mesosphere than in the stratosphere.

Mid-spring SSW spring transitions are characterized by an excess of $\overline{u}$ and NAM of −1.0 std at 10 and 0.3 hPa in April describing the final warming in the stratosphere and mesosphere. Thus, the final wind reversal to easterly winds occurs almost simultaneously at all levels in the stratosphere and mesosphere. This is also in contrast to the *early spring SSW* spring transitions where westerly winds occur again in the mesosphere after the final warming in the stratosphere. In contrast to the above described spring transitions, the

Table 1
Classification of Spring Transitions

Mid-winter SSW	Late-winter SSW	Early spring SSW	Mid-spring SSW	No negative NAM
1987	1980	1985	1982	1990
2001	1981	1986	1991	1993
2004	1983	1992	1995	1997
2006	1984	1994	1996	1998
2009	1988	2000	2003	2002
2013	1989	2005	2011	2007
2019	1999	2014	2015	2010
	2008	2016	2017	2012
	2018			2020

Abbreviations: NAM, Northern Annular Mode; SSW, sudden stratospheric warming.

time period of negative $\overline{u}$ and NAM is almost equally long in the stratosphere and mesosphere here. Note, that there can be minor warmings in the pre-winter in this spring transition class.

No negative NAM spring transitions exhibit a behavior similar to the average over all winter and springs months but also by a permanently positive NAM at 10 hPa. Thus, minor warmings can occur in the preceding winter or even major warmings with only a very weak easterly wind and a fast re-reversal to westerly winds in the stratosphere and mesosphere.

Summarizing, it is the date of occurrence of the SSW, the behavior of the stratosphere and mesosphere after the SSW and the structure of the final wind reversal in the middle atmosphere that are needed to uniquely classify a spring transition.

The MERRA-2 data set includes 41 springs whereby each is assigned to one of the five classes described above. Table 1 shows which spring transition is assigned to which class. Similar to Figure 1, the temporal-vertical evolution of the zonal mean zonal wind and NAM index for each of the 41 years can be found in the *supporting information* sorted by the five spring transition classes. Note, that we tested the manually generated classification and sorting of the spring transitions using self-organizing maps (Cassano et al., 2007) and got similar results (not shown). Note also, that the number of spring transitions is similar in each class indicating an uniform distribution of the five spring transition classes.

In order to illustrate the differences between the different spring transition classes we will explain the classification by means of ambiguously seeming spring transition years. In 2010 a major SSW occurred in late January and early February (Dörnbracket al., 2012, see Figure S6 in the SI), making it a candidate for the *mid-winter SSW* spring transition. But, the weak and short negative NAM at 10 hPa as well as the weaker westerly zonal winds and positive NAM at 0.3 hPa ($std(\overline{u}), NAM < 1\ std$) prevented this classification. The recovery of the polar vortex after the SSW resulted in over 40 ms^{-1} weaker winds in 2010 compared to 2013. Finally, there was no late SFW occurring first at 1 hPa. In addition, there was another major SSW in mid-March, which had the potential to finally reverse the zonal wind in the stratosphere as in the *early spring SSW* spring transition class. However, compared to the *early spring SSW* spring transition, the negative NAM index associated with this SSW was too weak and not downward propagating.

In 2002 a major SSW occurred in February making it a candidate for the *late-winter SSW* spring transition (see Figure S6). However, this SSW barely reached 10 hPa and was thus much stronger in the mesosphere than in the stratosphere. Additionally, after the SSW $std(\overline{u})$ and NAM exceeded +1.0 std for less than 20 days and thus much too short to be classified as *late-winter SSW* spring transition. Since no other SSW occurred after the major SSW in February 2002, this year was classified as *No negative NAM* spring transition.

The winter 2020 (see Figure 1) was characterized by an unusually strong and persistent stratospheric polar vortex (Lawrence et al., 2020). Nevertheless, a quite strong minor warming occurred in mid-March, which would have had the potential to finally reverse the zonal wind and thus classifying it as *late-spring SSW* spring transition. However, due to the strong zonal winds in the stratosphere and the missing of a downward propagating NAM, this SSW had no significant impact on the final wind reversal in the middle stratosphere and thus it is finally classified as *No negative NAM* spring transition. In both 1994 and 1995 (see Figures S3 and S4 in the SI) the final wind reversal occurred around day 95 at 10 hPa. However, while 1994 is classified as *early spring SSW* spring transition, 1995 is classified as *mid-spring SSW* spring transition. The difference is a 10 day long westerly wind bubble above 58 km between day 96 and 106 and the shorter time period of $std(\overline{u}), NAM < -1\ std$ at 0.3 hPa than at 10 hPa.

These examples show the importance of the downward propagating negative NAM index and the behavior of the stratosphere and mesosphere after SSWs in our definition of the spring transition classes.

To compare the new spring transition classes with other studies using other classifications, Figure 2 shows the temporal range of the days where the final zonal wind reversal of the different classes occurs in the

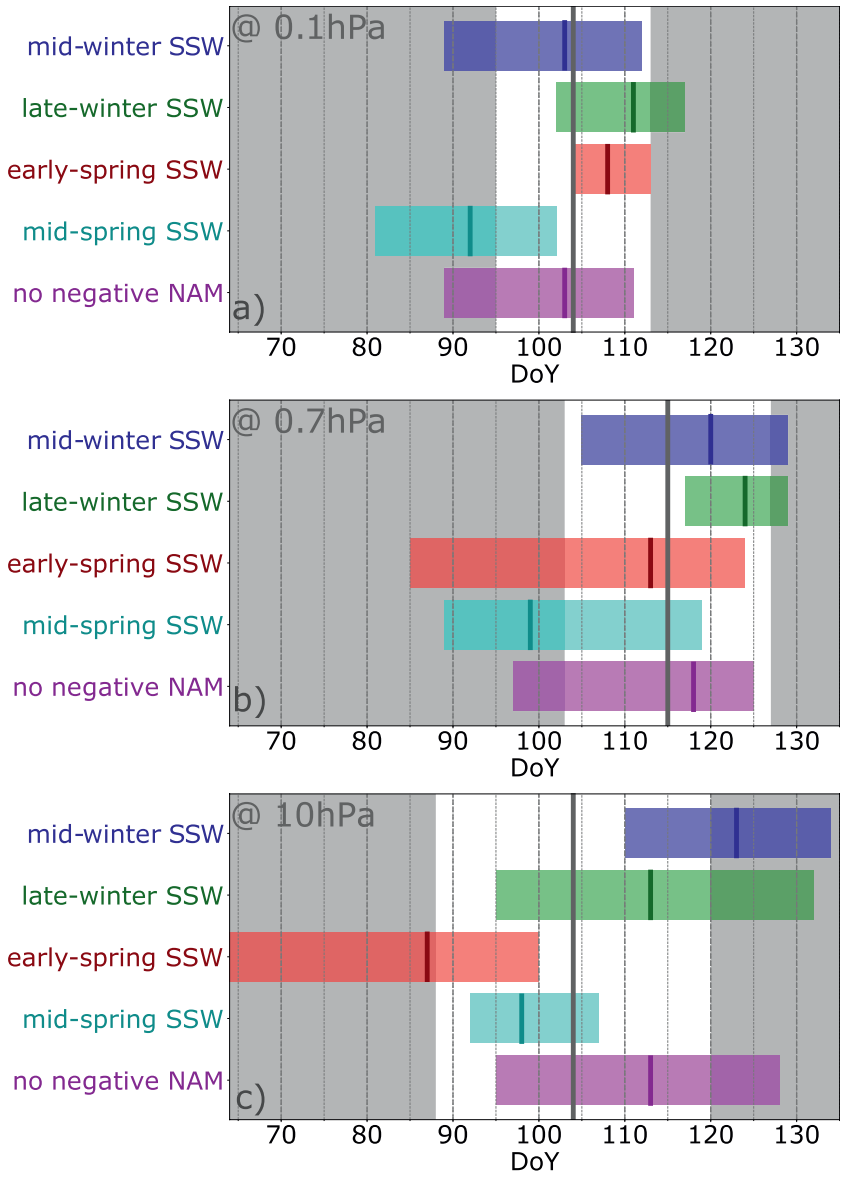

Figure 2. The colored bars represent the time period in which the respective spring transition class occurred between 1980 and 2020 at the pressure levels (a) 0.1 hPa, (b) 0.7 hPa, and (c) 10 hPa. The small vertical line in each bar gives the mean day of onset of the respective class. The vertical gray line represents the climatological (all 41 years) onset of the spring transition and the gray background the time period where one standard deviation is exceeded for each pressure level separately.

41 available spring transitions. Thus, the beginning and end of the colored bars represent the earliest and latest final wind reversal observed in the corresponding spring transition class. This is shown for three different pressure levels (10, 0.7, and 0.1 hPa). The 10 hPa level was chosen to compare our results with other existing studies, the 0.7 hPa level was chosen because in some years it is the level where the wind reverses the latest, and 0.1 hPa was chosen to represent the mesospheric spring transition. Following the common early late classification, the dark gray line represents the average day of final wind reversal over all 41 spring transitions at each level while the white region represents the 1-sigma interval. Thus, the gray shaded area represents the days where one standard deviation from this average day of final wind reversal is exceeded. Therefore, spring transition classes, in which the colored bars reach into the gray area, are more likely included in the common early late classification especially when their average day of wind reversal (darker colored line within the bars) lies outside the one-standard deviation interval of the overall mean

(white area) and thus within the gray shaded area. This enables us a better comparison between the new classification and the common early late classification.

On average (long vertical gray lines), the final wind reversal occurs simultaneously at 10 hPa and 0.1 hPa but the standard deviation is much smaller in the mesosphere than in the stratosphere. At 0.7 hPa the average spring transition occurs 11 days later than in the two pressure levels above and below and its standard deviation is smaller than in the stratosphere, but larger than in the mesosphere. Note, that the average spring transition day at 10 hPa and its standard deviation is in agreement with other studies (Ayarzagüena & Serrano, 2009; Black et al., 2006; Butler et al., 2019; Kelleher et al., 2020; Li et al., 2012; Wei, 2007).

On average (small vertical colored lines) *mid-winter SSW* spring transitions (dark blue) occur first in the mesosphere and propagate downward within 20 days to the middle stratosphere. While they occur almost at the climatological spring transition onset day in the mesosphere, they occur later in the levels below. At 10 hPa they even exceed the standard deviation and thus contribute to the late SFW in other studies (Butler et al., 2019; Wei, 2007).

Late-winter SSW spring transitions (green) occur also first in the mesosphere, a few days later in the stratosphere and at last in the stratopause region. At all levels the spring transition takes place later than the overall average but does not exceed one standard deviation. Thus, most spring transitions of this class are not considered when the standard classification with early and late SFW is applied. However, the temporal range, in which the spring transitions occur, is much wider in the stratosphere (∼40 days) than in the other two upper levels (10–15 days).

The final wind reversal in the *early spring SSW* spring transitions (red) occurs on average first in the middle stratosphere, over 20 days later in the mesosphere and finally in the stratopause region. This class is the only class exceeding the minus one standard deviation with respect to the climatology at 10 hPa. Thus, this class is the only one contributing to the so called early SFW. The temporal range, in which these spring transitions occur, is quite large in the lower two levels (∼35 days) and extremely narrow in the mesosphere (∼9 days).

Mid-spring SSW spring transitions (light blue) occur first in the mesosphere and almost simultaneously in the middle and upper stratosphere. They occur at all levels before the corresponding climatological onset day but never exceed the standard deviation at 10 hPa. Additionally, the temporal range, in which these spring transitions occur, is with 15 days the narrowest at 10 hPa and thus do neither contribute to the early nor to the late SFWs.

No negative NAM spring transitions occur on average similar to the *late-winter SSW* spring transitions first in the mesosphere, then in the stratosphere and at last in the stratopause region but in general a little bit earlier than *late-winter SSW* spring transitions. The average onset day of this spring transition class lies within the standard deviation and thus this class contributes only little to the late SFWs.

Summarizing, only the *early spring SSW* spring transition class contributes to the early SFWs defined at 10 hPa, while the *mid-winter SSW* spring transition class strongly and the classes *late-winter SSW* and *no negative NAM* partly contribute to the late SFW. Note, the *mid-winter SSW* spring transitions seem to have the largest impact since their average onset day exceeds the standard deviation. The *mid-spring SSW* spring transition class does not contribute to either of these SFW classes. Our results agree well with findings of Hu et al. (2015) that SFWs are delayed when a minor or major SSW occurs in the preceding winter which is fulfilled for the spring transition classes *mid-winter SSW*, *late-winter SSW* and *no negative NAM*.

Using the classification of 10 hPa-first and 1 hPa-first, the *mid-winter SSW* spring transition is the only one contributing on average to the 1 hPa-first class. The *late-winter* and *early spring SSW* as well as the *no negative NAM* spring transition contribute to the 10 hPa-first class. The *mid-spring SSW* spring transition class does not contribute to either of this vertically defined SFWs classes. These results agree well with findings of Thiélemont et al. (2019) that SSWs occurring in mid-winter favor a 1 hPa-first SFW while SSWs occurring in late winter favor a 10 hPa-first SFW. However, they also found that winters without a SSW are followed by 1 hPa-first SFW which we cannot confirm with our analysis. One possible explanation for this discrepancy may be that Thiélemont et al. (2019) used model data (CESM/WACCM) that include significantly less 10 hPa-first SFW events compared to ERA-Interim. However, we also note, that for single cases the

10 hPa-first and 1 hPa-first classification might be different especially for the *no negative NAM* spring transition where the average onset days at 10 and 0.7 hPa are close together. This also shows the partly strong mixture of different spring transition types in the classes defined in previous studies.

3.3. Average Characteristics of the Spring Transition Classes

Using composite analysis, the average characteristics of the five spring transition classes are investigated. Thus, time periods and regions can be identified that might enable a prediction of the spring transition type and onset day already in winter and thus contributing to the seasonal to subseasonal forecast.

Similar to Figure 1, Figure 3 now shows, the composite of the zonal mean zonal wind (left) and NAM index (right) for each spring transition class (rows). The stippling shows significant values obtained by a bootstrap method ($p < 0.05$, see Section 2.4). The spring transition class *mid-winter SSW* (Figures 3a and 3f) is on average characterized by a very weak and even reversed zonal wind in January and February whereby the weakening first occurs between 20 and 60 km and then propagates downward with time. Thus, this spring transition class is characterized by a major SSW starting sometime in January. The weak zonal wind is accompanied by a strong negative NAM index also propagating downward with time. After the SSW a strong polar vortex forms in the middle mesosphere, which propagates downward with time and is accompanied by a strong positive NAM index. All these characteristics are significant distinguishing this class from the other classes and thus enable a prediction of the spring transition onset day and type already in mid-winter. The final wind reversal starts in mid-April in the mesosphere, propagates downward to the stratopause region and happens then simultaneously at all stratospheric levels.

The vertical and temporal structure of the *late-winter SSW* spring transition (Figures 3b and 3g) is similar in zonal wind and NAM index behavior to *mid-winter SSW* spring transitions, but occurs approximately 30 days later in the year and with a weaker magnitude. Note, that the downward propagating positive NAM is not as pronounced as for *mid-winter SSW* spring transitions. The final wind reversal of the *late-winter SSW* spring transitions is similar to the *mid-winter SSW* spring transitions in the mesosphere, but differs in the stratosphere. Here, the final wind reversal starts around 30 km and then propagates downward to the lower stratosphere and upward to the stratopause. Thus, the final wind reversal in the mesosphere is somewhat decoupled from that in the stratosphere.

The structure of the *early spring SSW* spring transition (Figures 3c and 3h) is again similar to *mid-winter SSW* spring transitions, but occurs now approximately 50 days later in the year and with an even weaker magnitude. However, even though the polar vortex forms in mesosphere again with an even weaker magnitude compared to *late-winter SSW* spring transitions, the zonal wind remains easterly in the stratosphere resulting in a very early spring transition in that region. In the mesosphere, the final wind reversal occurs at least one month later than in the stratosphere and propagates downward with time indicating a dominance of radiative forcing for this spring transition class. Thus, the final wind reversal in the mesosphere is again somewhat decoupled from that in the stratosphere.

The spring transition class *mid-spring SSW* (Figures 3d and 3i) is on average characterized by a weakened zonal wind at the end of January/beginning of February indicative of a minor mid-winter SSW and accompanied by a negative NAM index which is not downward propagating. At the beginning of April, and thus 70 days later as in the *mid-winter SSW* spring transition class, a major SSW occurs, traditionally classified as a final warming, finally reversing the zonal wind at all altitude almost simultaneously. This SSW is again accompanied by a downward propagating negative NAM. In the recovery phase of the SSW, the easterly winds weaken again but never reverse back to winter westerly winds at any altitude.

Thus, the above described four spring transition classes have in common that a major SSW occurs at any point in time which is accompanied by a negative downward propagating NAM.

The fifth class, *no-negative NAM* spring transition (Figures 3e and 3j), is on average characterized by a non-significant weakening of the zonal wind and NAM index at the end of February, indicative for a minor SSW in the upper stratosphere and mesosphere. Significant positive zonal wind and NAM values can only be found after February in the lower and middle stratosphere. The final wind reversal propagates irregularly downward in the mesosphere and occurs first around 35 km in the stratosphere, while it is upward

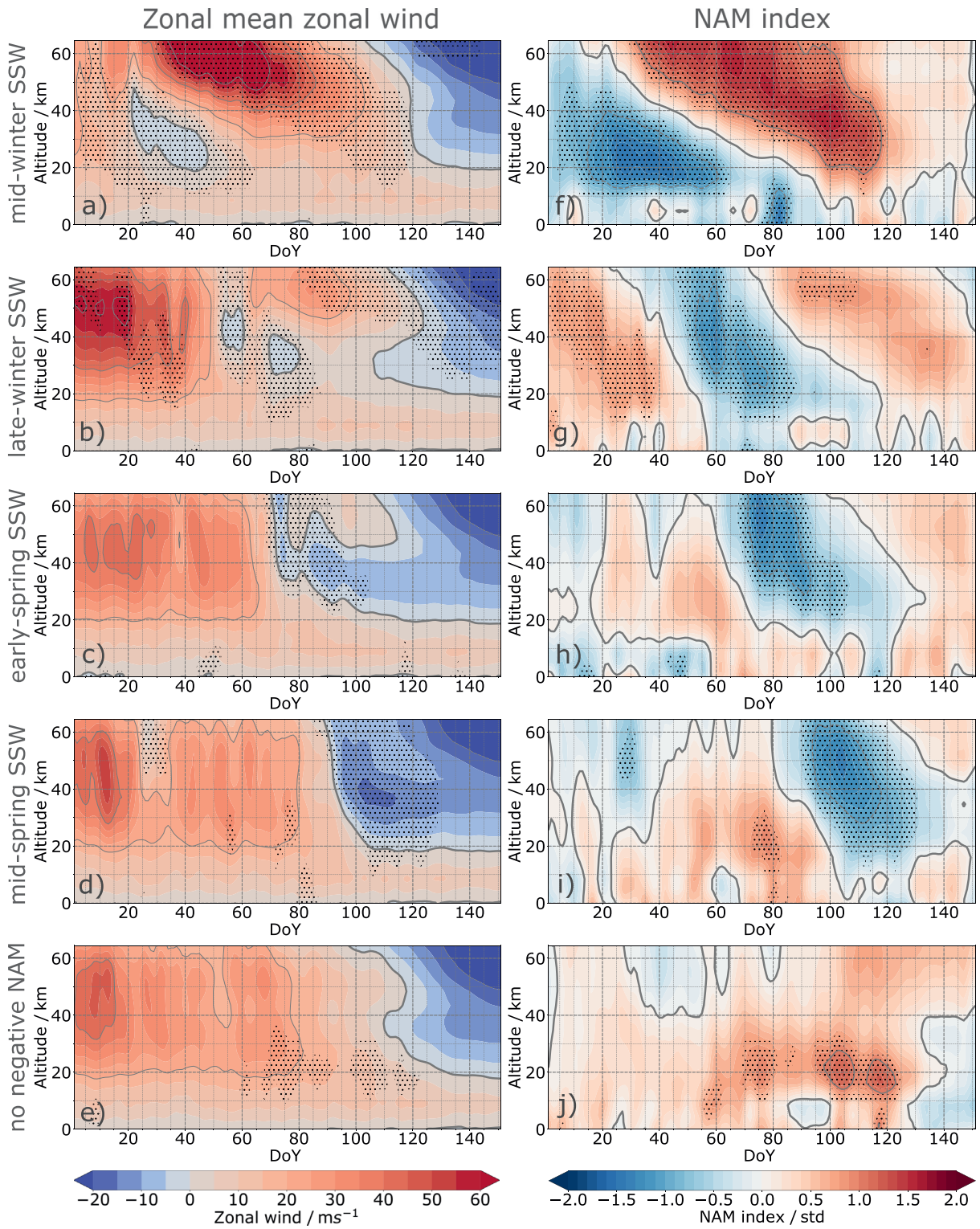

Figure 3. Time-height cross-sections of the composites of the zonal mean zonal wind averaged between 60° and 70°N (left) and NAM index (right) for the different spring transition classes (a–e) derived from MERRA-2 data. The stippling shows significant values ($p < 0.05$, see Section 2.4). NAM, Northern Annular Mode.

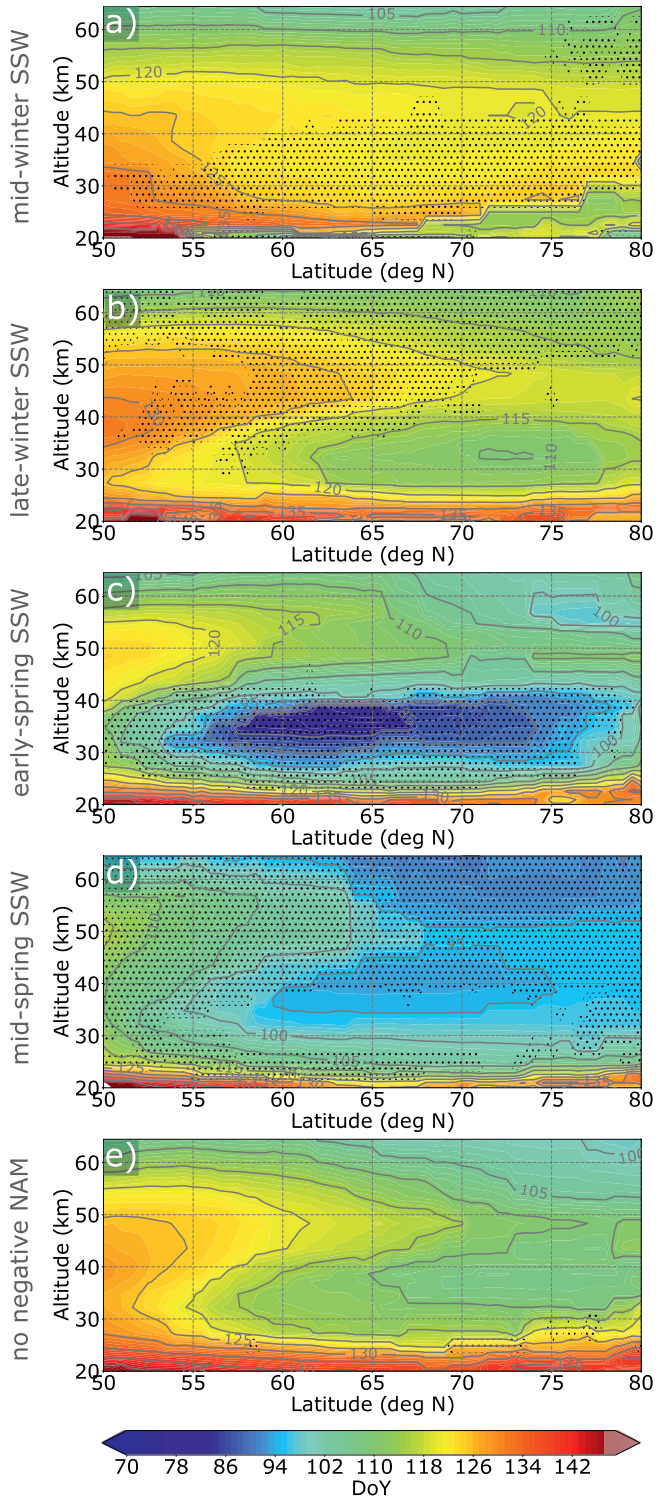

Figure 4. Latitude-height cross-sections of the average spring transition onset day for each spring transition class (a–e) derived from MERRA-2 data. The stippling shows significant values ($p < 0.05$).

propagating above and downward propagating below, each also irregularly. Thus, the final wind reversal in the mesosphere is again somewhat decoupled from that in the stratosphere. Remarkable about this class is the missing of a major SSW accompanied by a downward propagating negative NAM. Note, that the stippling in the lower stratosphere in March and April mostly originates from the year 2020 where the polar vortex was the strongest and most persistently cold in over 40 years (Lawrence et al., 2020).

3.4. Average Latitude-Altitude Structure of the Spring Transition Onset Day

Our definition of the spring transition, which is in accordance with other studies (Butler et al., 2019; Hu, Ren, Yu, & Xu, 2014; Wei, 2007), uses the zonal mean zonal wind averaged between 60° and 70°N. However, we are also interested in the average latitudinal-altitudinal structure of the different spring transitions in the middle atmosphere. Therefore, Figure 4 shows the latitude-altitude cross-section of the mean day when the zonal mean zonal wind finally reverses, calculated at each location separately. One feature that occurs in all spring transitions, is a tongue of relatively late wind reversal approximately at 40–50 km and between 50° and 70°N. Apart from this tongue, the *mid-winter SSW* spring transitions (Figure 4a) are solely downward propagating, whereby it is faster in the stratosphere than in the mesosphere. For *late-winter SSW* spring transitions (Figure 4b) the earliest wind reversal occurs poleward of 60°N in the middle stratosphere with its center between 70° and 75°N at 32 km. The mesospheric wind reversal is in general downward propagating but occurs earlier poleward of 70°N due to the more pronounced tongue of later wind reversal in the upper stratosphere/lower mesosphere. For *early spring SSW* spring transitions (Figure 4c), the earliest wind reversal occurs poleward of 50°N in the middle and upper stratosphere with its center between 57° and 67°N around 37 km. There is a second area with early wind reversal poleward of 70°N above the stratopause. *Mid-spring SSW* spring transitions (Figure 4d) occur almost simultaneously at all altitudes poleward of 65°N. Southward of that, the tongue of later wind reversal prevents an earlier onset of the spring transition. Nevertheless, the onset days within this tongue are the earliest compared to the other spring transition classes. The final wind reversal in the *no-negative NAM* spring transitions (Figure 4e) occurs first in the mesosphere northward of 70°N and propagates downward with time. There is a second area with early wind reversal in the middle and upper stratosphere poleward of 65°N from where the spring transition propagates downward and especially equatorward. The tongue of later wind reversal is also quite pronounced, but less than for *late-winter SSW* spring transitions.

Thus, there are sometimes latitudinal differences in the spring transitions in the stratosphere and mesosphere indicating that latitudinally differentiating studies might be worth to be carried out, but are beyond the scope of this study. However, our choice of averaging between 60° and 70°N covers the main features of each class.

3.5. Main Forcing of the Spring Transition Classes

The timing and dynamical evolution of a spring transition is influenced by a combination of radiative forcing and planetary wave forcing effects.

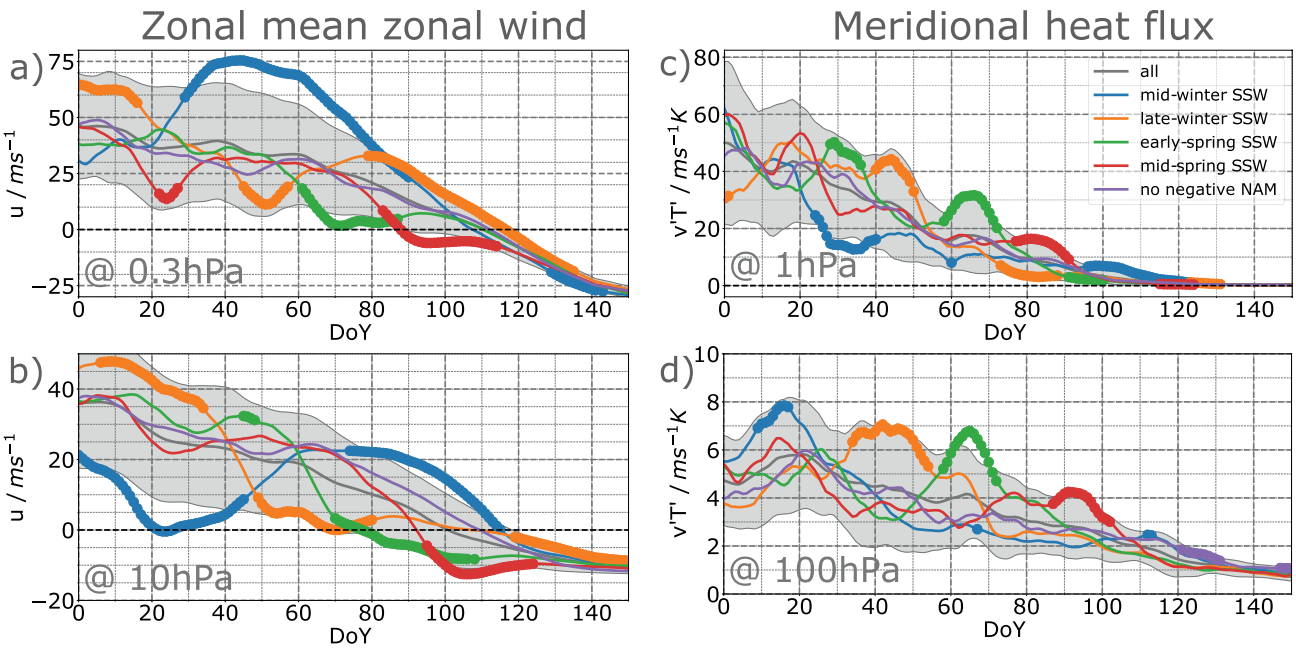

Figure 5. Average temporal evolution of the zonal mean zonal wind averaged between 60° and 70°N at (a) 0.3 hPa and (b) 10 hPa and of the meridional heat flux averaged between 40° and 75°N at (c) 1 hPa and (d) 100 hPa for the different spring transition classes (colored lines). Colored dots represent significant values ($p < 0.05$) for the respective class. The gray line represents the climatology (all 41 years) and its standard deviation (gray shading).

In the next paragraph we want to investigate to what extent PWs have an impact on the stratospheric and mesospheric final wind reversal for the different spring transition classes. Therefore, Figure 5 shows the average temporal evolution of the zonal wind in the stratosphere and mesosphere and meridional heat flux ($v'T'$, a measure of wave activity) in the middle and upper stratosphere. The different spring transition classes are represented by the colored lines whereby dots denote significant values.

In general, the zonal winds as well as the meridional heat fluxes decrease from mid-winter to late spring in the stratosphere and mesosphere (Figure 5 gray line). The SSWs, the occurrence time of which defines the different spring transition classes, are all characterized by significantly strong heat fluxes (around DoY: 18, 42, 65, 85, –) followed by significantly weak zonal winds (around DoY: 22, 55, 75, 95, –) in the stratosphere and mesosphere (Figures 5c and 5d).

Mid-winter SSW spring transitions (blue line) are characterized by a significantly weak heat flux into the mesosphere around day 30 after the major SSW in January, leading to unusually strong winds (DoY 30–90) in that region. These stronger zonal winds propagate downward with time reaching the stratosphere shortly before the final wind reversal (DoY 75–110) accompanied with a weakly increased, but not significant, heat flux (at DoY 112). Thus, the final wind reversal of the *mid-winter SSW* spring transitions is primarily driven by radiative processes in both the stratosphere and mesosphere.

Late-winter SSW spring transitions (orange line) are characterized by a significantly weak heat flux into the mesosphere around day 80 after the major SSW in February, leading to significantly stronger winds in the mesosphere (DoY 80–130) shortly before the final wind reversal. At the same time the stratospheric zonal wind is weak (DoY 90–110; although not significant) so that the weak heat flux (DoY 80–100) can easily reverse the zonal wind at any time. Thus, the final wind reversal of *late-winter SSW* spring transitions is primarily driven by radiative processes in the mesosphere, while radiative and dynamical processes seem to equally influence the final wind reversal in the stratosphere.

Early spring SSW spring transitions (green line) are characterized by significantly strong heat fluxes into the stratosphere and mesosphere around day 65 before the SSW in March and thus also before the final wind reversal in the stratosphere. However, the mesospheric wind recovers (DoY 90–110) due to significantly weak heat fluxes (DoY 80–100) into the mesosphere resulting in a dominance of radiative processes which

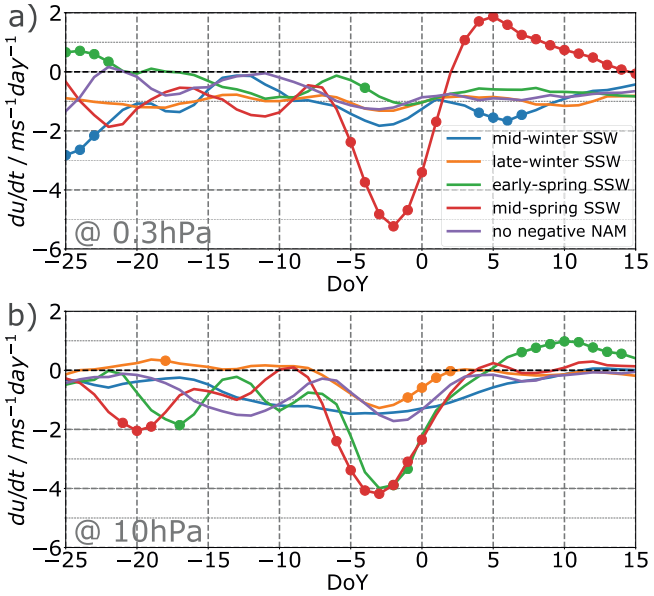

Figure 6. Average temporal evolution of the velocity of wind change per day centered around the spring transition onset day at (a) 0.3 hPa and (b) 10 hPa for the different spring transition classes (colored lines). Colored dots represent significant values ($p < 0.05$) for the respective class.

are still in winter mode due to the seasonal changes in the solar radiation. Thus, the final wind reversal of the *early spring SSW* spring transitions is primarily driven by dynamical processes in the stratosphere while radiative processes dominate in the mesosphere.

Mid-spring SSW spring transitions (red line) are characterized by significantly strong heat fluxes into the stratosphere and mesosphere (DoY 70–100) leading to a final wind reversal in both regions a few days later (DoY 85–95). Thus, this spring transition class is primarily dynamically driven in the stratosphere and mesosphere.

No-negative NAM spring transitions (purple line) mostly follow the climatology in the stratosphere and mesosphere so there are no significant values. Thus, the final wind reversal of this spring transition class is driven by a mixture of radiative and dynamical processes in the stratosphere and mesosphere. However, dynamical processes might dominate slightly given by the irregular structure of the zero wind line in Figure 3e) but this can differ from year to year.

Thus, early stratospheric final warmings, which are mostly driven by dynamical processes (Wei, 2007; Hu, Ren, Yu, & Xu, 2014), are here represented by *early spring SSW* spring transitions (cf. Figure 2). Late SFWs, which are mostly driven by radiative processes (Wei, 2007; Li et al., 2012; Hu, Ren, Yu, & Xu, 2014), are here mainly but not exclusively represented by *mid-winter SSW* spring transitions (cf. Figure 2). One hPa-first SFWs, which are mostly driven by radiative processes (Hardiman et al., 2011; Thiélemont et al., 2019), are here mainly but not exclusively represented by *mid-winter SSW* spring transitions (cf. Figure 2). And 10 hPa-first SFWs, which are mostly driven by dynamical processes (Hardiman et al., 2011; Thiélemont et al., 2019), are here represented especially by *early spring SSW* spring transitions but also by *late-winter SSW* spring transition and some of the *no negative NAM* spring transitions. Thus, our results regarding the dominance of radiative or dynamical processes leading to the final wind reversal in the stratosphere and mesosphere in the different spring transition classes agree well with previous studies. Note, that on average *mid-spring SSW* spring transitions are mostly not considered by these two standard classifications since its average occurrence time period does not exceed the standard deviation in the stratosphere (cf. Figure 2c) and it occurs almost simultaneously at all altitudes. Thus, our new classification and results give a more detailed view on the processes leading to the different types of spring transitions in the stratosphere *and* mesosphere possibly enabling a better prediction of when and how a spring transition takes place.

Another indicator, if a spring transition is driven by dynamical or radiative processes, is the speed of the transition from westerly to easterly winds. Slow transitions with less than 2 ms^{-1} per day are mostly driven by radiative processes, while fast transition with more than 3 ms^{-1} per day are mostly dynamically driven (Butler et al., 2019; Wei, 2007). Figure 6 shows the average temporal evolution of the velocity of wind change per day for the different spring transition classes, this time centered around the final wind reversal day in the stratosphere and mesosphere. In the stratosphere (see Figure 6b) the zonal wind decreases with up to 4 ms^{-1} per day in the week before the final wind reversal at day 0 for *early spring SSW* (green line) and *mid-spring SSW* spring transitions (red line). Thus, there is a fast transition for these two spring transition classes. The zonal wind decrease in the other three classes does not exceed the 2 ms^{-1} per day and thus, it is slow. These results agree well with findings of Wei (2007) and Butler et al. (2019) that early SFWs are fast, here represented by *early spring SSW* spring transitions, and that late SFW are slow, here represented mostly by *mid-winter SSW* spring transitions.

In the lower mesosphere (see Figure 6a) the only class, where the zonal wind decrease exceeds the threshold of 2 ms^{-1} per day, is the *mid-spring SSW* spring transition. The other four classes are characterized by a slow transition from westerly to easterly winds indicating a dominance of radiative processes in the mesosphere and agreeing to the results of Figure 5.

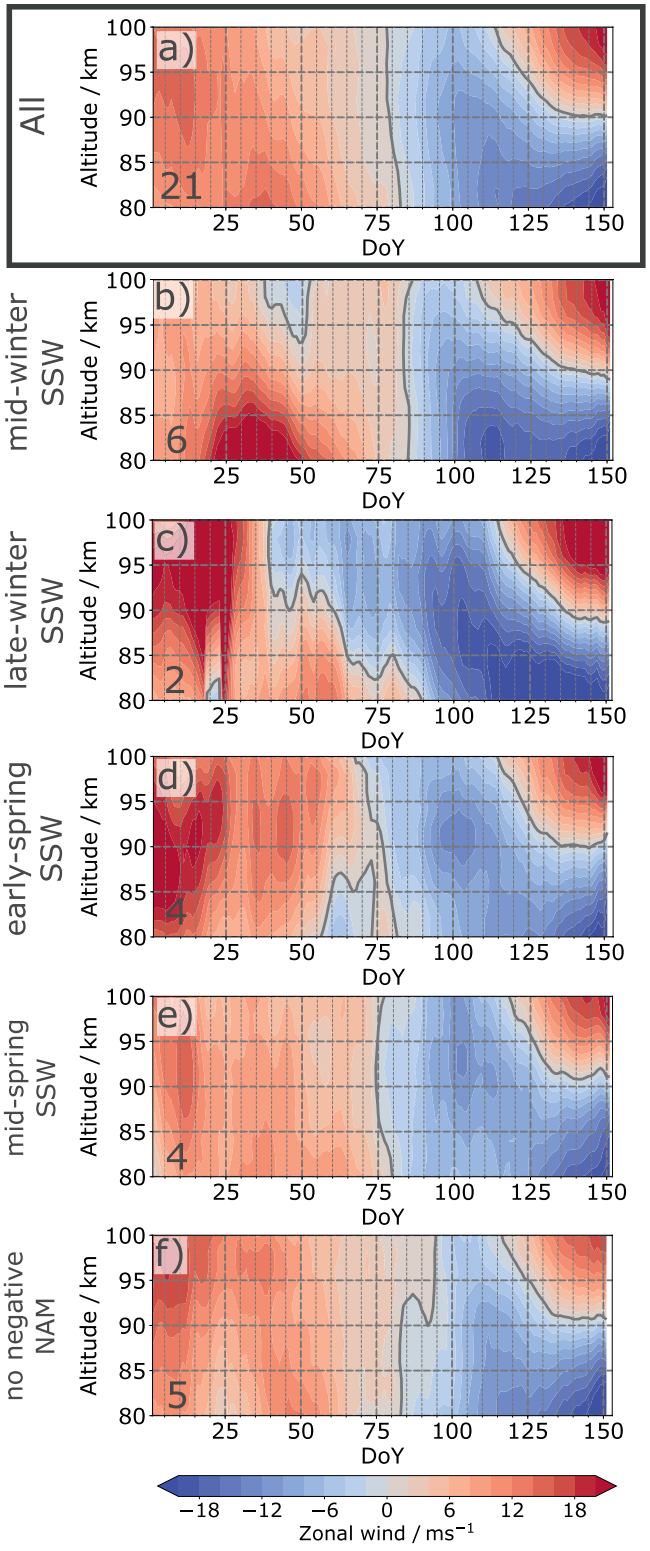

Figure 7. Composites of zonal wind of all available years (a) and for the different spring transition classes (b–f) derived from merged meteor radar data at Esrange (68°N, 21°E) and Sodankylä (67°N, 26°E). The numbers in the lower left corners represent the number of spring transitions included in the respective composite.

Concluding, we introduced five new spring transition classes which already include the occurrence, timing and strength, which is given by the NAM index, of a major SSW in winter and spring. This improves our understanding of spring transition processes and thus might improve the prediction of stratospheric final warmings. Especially the *mid-winter SSW* spring transition class is a good candidate to be predicted already in January when one also takes the zonal wind in the mesosphere into account (see Figure 5a). These results show the importance of global mesospheric observations as for example given by MLS and reanalysis data like MERRA-2 that are available beyond the stratopause as also shown by McCormack et al. (2017).

4. Spring Transition in the MLT

In this section average characteristics of the different spring transition classes in the MLT are discussed as well as their impact on the variability of the upper MLT and ionosphere.

In the MLT the wind reversal from westerly to easterly wind at the end of the winter represents the beginning of spring, while the renewed wind reversal from easterly to westerly wind approximately 60 days later represents the beginning of summer (Hoffmann et al., 2010; Merzlyakov et al., 2012). Figure 7 shows the composites of the zonal wind in the MLT for the merged Esrange (68°N, 21°E) and Sodankylä (67°N, 26°E) data set for all available years (a) as well as for the different spring transition classes (b–f). On average, the zonal wind reverses between day 78 at 90 km and 83 at 80 km in the MLT in spring (see Figure 7a), which is in agreement with Merzlyakov et al. (2012). There is a slightly downward propagation of the wind reversal between 100 and 80 km within 5 days indicating that radiative as well as dynamical processes play a role.

Note, that due to the shorter observation periods of the radar compared to MERRA-2 data, the following statements can only be treated as indications. Nevertheless, tendencies of how the MLT behaves during the different spring transition classes can be seen.

The zonal wind in the MLT in the *mid-winter SSW* spring transition (Figure 7b) is characterized by strong zonal winds below 90 km after the SSW, which is in agreement with our composite results obtained from MERRA-2 in Figure 3. The wind reversal occurs later than in the climatology probably induced by the strong winds after the SSW, which prohibits planetary wave propagation from below (Charney & Drazin, 1961). Thus, the spring transition seems to be more radiatively driven but the impact of dynamical processes cannot be ruled out as the reversal happens simultaneously at all altitudes.

The zonal wind in the MLT in the *late-winter SSW* spring transition (Figure 7c) is characterized by strong zonal winds above 90 km before the SSW. The spring time wind reversal above 85 km occurs much earlier (up to 40 days) than in the climatology, probably induced by the SSW or at least by dynamical processes, while the wind reversal below 85 km continuously propagates downward indicating a dominance of radiative processes. Note, that these observations should be treated with caution since only two events are included in this composite.

The zonal wind in the MLT in the *early spring SSW* spring transition (Figure 7d) is characterized by strong zonal winds in January. The spring time wind reversal occurs on average earlier than in the climatology and the downward propagation is slower. However, in 2016 the SSW occurred extremely early in spring (Manney & Lawrence, 2016) finally reversing the zonal wind simultaneously at all altitudes in the MLT (cf. Figure 1c). Thus, on average this MLT spring transition is radiatively driven at all altitudes but exceptions with a dominating dynamical process can occur.

On average the *mid-spring SSW* spring transition (Figure 7e) wind reversal occurs slightly earlier than in the climatology and almost simultaneously at all levels in the MLT. However, individual events show that the vertical structure of the wind reversal depends on the timing of the mid-spring SSW. If the SSW occurs early within the *mid-spring SSW* spring transition time range (see Figure 2) then the wind reversal is dynamically driven and occurs simultaneously at all MLT levels, but if the SSW occurs later, the wind reverses already in the MLT region driven by radiative processes and the easterly wind just strengthens for the duration of the SSW (not shown).

The wind reversal in the *no negative NAM* spring transition (Figure 7f) occurs especially above 90 km up to 20 days later than in the climatology. For individual events a wave-like structure occurs before the spring time wind reversal postponing the final wind reversal. This indicates a mixture of radiative and dynamical processes leading to the spring transition in the MLT.

Summarizing, the wind reversal in the MLT occurs between end of March and beginning of April and shows distinctively less variability between the spring transition classes compared to the stratosphere and lower mesosphere, which agrees well with findings of Merzlyakov et al. (2012). In general, the wind reversal propagates downward indicating that the main drivers are radiative processes, but since the speed of the downward propagation varies between the spring transition classes also dynamical processes seem to play a role (Aushev et al., 2006; Merzlyakov et al., 2012).

Yamazaki and Matthias (2019) found in some years a strong 10-day wave during spring in the MLT generated by instabilities in the stratosphere. Comparing their results with ours it can be seen that this strong 10-day wave occurs only in the spring transition classes *early spring SSW* and *mid-spring SSW*. However, such waves occur rather rarely in association with mid-winter SSWs and if so with a weaker magnitude (Yamazaki & Matthias, 2019). Thus, it seems that a SSW occurring in the already weakened winter circulation (due to the changes in the solar zenith angle) is necessary to induce baroclinic instabilities leading to the long period planetary waves observed in the MLT. When these waves modulate the amplitude or phase of the solar tides in the MLT (Yiğit & Medvedev, 2015), planetary wave-like oscillations can migrate even into the F-region (Borries & Hoffmann, 2010; Gordienko et al., 2007) disturbing the ionosphere there. This can in turn affect radio communication and GPS signals. Thus, with the new and more detailed definition of the spring transition classes, that already includes the mid-winter conditions, a better prediction of the MLT and ionosphere variability might be possible in spring.

5. Summary and Conclusion

This study introduces a new classification of the spring transition in the middle atmosphere based on the vertical-temporal development of the zonal mean zonal wind and NAM index in the core region of the polar vortex beginning already in January. There are five new classes defined by the occurrence and timing of a SSW in association with a negative downward propagating NAM index lasting for several weeks as described in Baldwin and Dunkerton (2001). The average characteristics of the five classes were investigated using MERRA-2 reanalysis data showing that the timing of the SSW has an impact on the timing and vertical structure of the final wind reversal, not only in the stratosphere but also in the mesosphere. The characteristics of the five new spring transition classes and their affiliation to commonly used classifications are summarized in Table 2. The new knowledge enables us to improve our understanding of the spring transition processes and shows us the importance of mesospheric observations. Two of the classes (early- and mid-spring SSW spring transitions) have a direct impact on the variability of the MLT (Yamazaki & Matthias, 2019) and thus maybe also on the ionospheric variability.

Table 2
Summary of the Average Characteristics of the New Spring Transition Classes and Their Affiliation to Commonly Used Classifications

	Mid-winter SSW	Late-winter SSW	Early spring SSW	Mid-spring SSW	No negative NAM
Major SSW	January	February	March	April	–
Negative NAM	✓	✓	✓	✓	–
Onset day at 10 hPa	123	113	87	98	113
Onset day at 1 hPa	121	124	112	97	118
Final wind reversal Stratosphere	simultaneously	up- and downward propagating from 10 hPa	simultaneously	simultaneously	up- and downward propagating from 6 hPa
Final wind reversal Mesosphere	downward propagating	downward propagating	downward propagating	simultaneously	downward propagating
Main forcing Stratosphere	radiative	radiative + dynamical	dynamical	dynamical	radiative +dynamical
Main forcing Mesosphere	radiative	radiative	radiative	dynamical	radiative +dynamical
Early/late	late	(late)	early	–	(late)
10 hPa/1 hPa-first	(1 hPa-first)	10 hPa-first	10 hPa-first	–	10 hPa-first

Abbreviations: NAM, Northern Annular Mode; SSW, sudden stratospheric warming.

This study is the first which systematically investigates the spring transition in the whole middle atmosphere and thus connecting the final wind reversal in the stratosphere and mesosphere. The expansion into the mesosphere not only improves our understanding but also might enable a better prediction of the spring transition. Additionally, the division into five classes spanning the middle atmosphere allows a more detailed characterization of the final wind reversal than earlier studies, which also improves our understanding of the spring transition. These results show the importance of global mesospheric observations.

For the prediction of the spring transition, exact thresholds are needed for the zonal wind and NAM index in winter in the stratosphere and mesosphere. Further studies are needed to investigate the latitudinal differences of the five classes, the prediction of the timing and type of the spring transition and the impact of the five different classes on our tropospheric weather as well as on the variability of the MLT region and ionosphere.

Data Availability Statement

The meteor radar data are available at https://www.sgo.fi/pub/JGR_SpringTrans_2020/.

Acknowledgments
We would like to thank the people at the National Aeronautics and Space Administration (NASA, USA) for providing MERRA-2 data and we downloaded from https://doi.org/10.5067/A7S6XP56VZWS. We thank the Jet Propulsion Laboratory/NASA for providing access to the Aura/MLS level 2 retrieval products downloaded from http://mirador.gsfc.nasa.gov. The authors would like to thank the MLS team for their effort in providing and continuously improving the high-quality data sets used in this study. The Esrange meteor radar operation, maintenance and data collection is provided by Esrange Space Center of Swedish Space Corporation. The meteor radar data analysis is supported by the ARISE2/ARISE-IA project (http://ARISE-project.eu, grant no. 653980) and received funding from the European Community's Horizon 2020 program. Gunter Stober is a member of the Oeschger Center for Climate Change Research. We thank Nick Mitchell for providing the meteor radar data from Kiruna. We also thank the anonymous reviewers for their constructive comments helping to improve this paper. Open access funding enabled and organized by Projekt DEAL.

References

Akiyoshi, H., & Zhou, L. B. (2007). Midlatitude and high-latitude N2O distributions in the Northern Hemisphere in early and late Arctic polar vortex breakup years. *Journal of Geophysical Research*, *112*(D18). https://doi.org/10.1029/2007JD008491

Aushev, V. M., Fedulina, I. N., Gordienko, G. I., López-González, M. J., Pogoreltsev, A. I., Ryazapova, S. S., & Shepherd, M. G. (2006). Springtime effects in the mesosphere and ionosphere observed at northern midlatitudes. *Planetary and Space Science*, *54*(6), 559–571. https://doi.org/10.1016/j.pss.2006.01.002

Ayarzagüena, B., & Serrano, E. (2009). Monthly characterization of the tropospheric circulation over the Euro-Atlantic area in relation with the timing of stratospheric final warmings. *Journal of Climate*, *22*(23), 6313–6324. https://doi.org/10.1175/2009JCLI2913.1

Baldwin, M. P., & Dunkerton, T. J. (2001). Stratospheric harbingers of anomalous weather regimes. *Science*, *294*(5542), 581–584. https://doi.org/10.1126/science.1063315

Baldwin, M. P., & Thompson, D. W. J. (2009). A critical comparison of stratosphere-troposphere coupling indices. *Quarterly Journal of the Royal Meteorological Society*, *135*(644), 1661–1672. https://doi.org/10.1002/qj.479

Baumgarten, K., & Stober, G. (2019). On the evaluation of the phase relation between temperature and wind tides based on ground-based measurements and reanalysis data in the middle atmosphere. *Annales Geophysicae*, *37*(4), 581–602. https://doi.org/10.5194/angeo-37-581-2019

Black, R. X., & McDaniel, B. A. (2007). The dynamics of northern hemisphere stratospheric final warming events. *Journal of the Atmospheric Sciences*, *64*(8), 2932–2946. https://doi.org/10.1175/JAS3981.1

Black, R. X., McDaniel, B. A., & Robinson, W. A. (2006). Stratosphere-troposphere coupling during spring onset. *Journal of Climate*, *19*(19), 4891–4901. https://doi.org/10.1175/JCLI3907.1

Borries, C., & Hoffmann, P. (2010). Characteristics of f2-layer planetary wave–type oscillations in northern middle and high latitudes during 2002 to 2008. *Journal of Geophysical Research*, *115*(A11). https://doi.org/10.1029/2010ja015456

Bosilovich, M., Lucchesi, R., & Suarez, M. (2015). *MERRA-2: File specification* (Technical Report). NASA GMAO Publications.

Butler, A. H., Charlton-Perez, A., Domeisen, D. I. V., Simpson, I. R., & Sjoberg, J. (2019). Predictability of northern hemisphere final stratospheric warmings and their surface impacts. *Geophysical Research Letters*, *46*(17–18), 10578–10588. https://doi.org/10.1029/2019GL083346

Butler, A. H., Sjoberg, J. P., Seidel, D. J., & Rosenlof, K. H. (2017). A sudden stratospheric warming compendium. *Earth System Science Data*, *9*(1), 63–76. https://doi.org/10.5194/essd-9-63-2017

Cassano, J. J., Uotila, P., Lynch, A. H., & Cassano, E. N. (2007). Predicted changes in synoptic forcing of net precipitation in large arctic river basins during the 21st century. *Journal of Geophysical Research: Biogeosciences*, *112*(G4). https://doi.org/10.1029/2006jg000332

Charney, J. G., & Drazin, P. G. (1961). Propagation of planetary-scale disturbances from the lower into the upper atmosphere. *Journal of Geophysical Research*, *66*(1), 83–109. https://doi.org/10.1029/jz066i001p00083

Dörnbrack, A., Pitts, M. C., Poole, L. R., Orsolini, Y. J., Nishii, K., & Nakamura, H. (2012). The 2009-2010 Arctic stratospheric winter—General evolution, mountain waves and predictability of an operational weather forecast model. *Atmospheric Chemistry and Physics*, *12*(8), 3659–3675. https://doi.org/10.5194/acp-12-3659-2012

Gelaro, R., McCarty, W., Suárez, M. J., Todling, R., Molod, A., Takacs, L., et al. (2017). The modern-era retrospective analysis for research and applications, version 2 (MERRA-2). *Journal of Climate*, *30*(14), 5419–5454. https://doi.org/10.1175/JCLI-D-16-0758.1

Gordienko, G. I., Fedulina, I. N., Altadill, D., & Shepherd, M. G. (2007). Upper ionosphere variability over Alma-Ata and Observatorio Del Ebro using the ΔfoF2 data obtained during the winter/spring period of 2003-2004. *Journal of Atmospheric and Solar-Terrestrial Physics*, *69*(17), 2452–2464. https://doi.org/10.1016/j.jastp.2007.05.008

Grotjahn, R., & Faure, G. (2008). Composite predictor maps of extraordinary weather events in the Sacramento, California, Region. *Weather and Forecasting*, *23*(3), 313–335. https://doi.org/10.1175/2007WAF2006055.1

Hardiman, S. C., Butchart, N., Charlton-Perez, A. J., Shaw, T. A., Akiyoshi, H., Baumgaertner, A., et al. (2011). Improved predictability of the troposphere using stratospheric final warmings. *Journal of Geophysical Research*, *116*(D18). https://doi.org/10.1029/2011JD015914

Hocking, W. K., Fuller, B., & Vandepeer, B. (2001). Real-time determination of meteor-related parameters utilizing modern digital technology. *Journal of Atmospheric and Solar-Terrestrial Physics*, *63*(2), 155–169. https://doi.org/10.1016/S1364-6826(00)00138-3

Hoffmann, P., Becker, E., Singer, W., & Placke, M. (2010). Seasonal variation of mesospheric waves at northern middle and high latitudes. *Journal of Atmospheric and Solar-Terrestrial Physics*, *72*(14), 1068–1079. https://doi.org/10.1016/j.jastp.2010.07.002

Hu, J., Ren, R., & Xu, H. (2014). Occurrence of winter stratospheric sudden warming events and the seasonal timing of spring stratospheric final warming. *Journal of the Atmospheric Sciences*, *71*(7), 2319–2334. https://doi.org/10.1175/JAS-D-13-0349.1

Hu, J., Ren, R., Xu, H., & Yang, S. (2015). Seasonal timing of stratospheric final warming associated with the intensity of stratospheric sudden warming in preceding winter. *Science China Earth Sciences*, *58*(4), 615–627. https://doi.org/10.1007/s11430-014-5008-z

Hu, J., Ren, R., Yu, Y., & Xu, H. (2014). The boreal spring stratospheric final warming and its interannual and interdecadal variability. *Science China Earth Sciences*, *57*(4), 710–718. https://doi.org/10.1007/s11430-013-4699-x

Karpechko, A. Y., Hitchcock, P., Peters, D. H. W., & Schneidereit, A. (2017). Predictability of downward propagation of major sudden stratospheric warmings. *Quarterly Journal of the Royal Meteorological Society*, *143*(704), 1459–1470. https://doi.org/10.1002/qj.3017

Kelleher, M. E., Ayarzagüena, B., & Screen, J. A. (2020). Interseasonal connections between the timing of the stratospheric final warming and Arctic Sea Ice. *Journal of Climate*, *33*(8), 3079–3092. https://doi.org/10.1175/JCLI-D-19-0064.1

Labitzke, K. (2000). Two lower Arctic stratosphere in winter since 1952. *SPARC Newsletter*, *15*, 11–14.

Lawrence, Z. D., Perlwitz, J., Butler, A. H., Manney, G. L., Newman, P. A., Lee, S. H., & Nash, E. R. (2020). The remarkably strong arctic stratospheric polar vortex of winter 2020: Links to record-breaking arctic oscillation and ozone loss. *Earth and Space Science Open Archive*, *27*. https://doi.org/10.1002/essoar.10503356.1

Li, L., Li, C., Pan, J., & Tan, Y. (2012). On the differences and climate impacts of early and late stratospheric polar vortex breakup. *Advances in Atmospheric Sciences*, *29*(5), 1119–1128. https://doi.org/10.1007/s00376-012-1012-4

Livesey, N. J., Read, W. G., Wagner, P. A., Froidevaux, L., Lambert, A., Manney, G. L., et al. (2015). *EOS MLS Version 4.2x Level 2 data quality and description document*. Jet Propulsion Laboratory, California Institute of Technology.

Lukianova, R., Kozlovsky, A., & Lester, M. (2018). Climatology and inter-annual variability of the polar mesospheric winds inferred from meteor radar observations over Sodankylä (67N, 26E) during solar cycle 24. *Journal of Atmospheric and Solar-Terrestrial Physics*, *171*, 241–249. https://doi.org/10.1016/j.jastp.2017.06.005

Lukianova, R., Kozlovsky, A., Shalimov, S., Ulich, T., & Lester, M. (2015). Thermal and dynamical perturbations in the winter polar mesosphere-lower thermosphere region associated with sudden stratospheric warmings under conditions of low solar activity. *Journal of Geophysical Research: Space Physics*, *120*(6), 5226–5240. https://doi.org/10.1002/2015JA021269

Manney, G. L., & Lawrence, Z. D. (2016). The major stratospheric final warming in 2016: Dispersal of vortex air and termination of arctic chemical ozone loss. *Atmospheric Chemistry and Physics*, *16*(23), 15371–15396. https://doi.org/10.5194/acp-16-15371-2016

Matthias, V., & Ern, M. (2018). On the origin of the mesospheric quasi-stationary planetary waves in the unusual arctic winter 2015/2016. *Atmospheric Chemistry and Physics*, *18*(7), 4803–4815. https://doi.org/10.5194/acp-18-4803-2018

McCormack, J., Hoppel, K., Kuhl, D., de Wit, R., Stober, G., Espy, P., et al. (2017). Comparison of mesospheric winds from a high-altitude meteorological analysis system and meteor radar observations during the boreal winters of 2009-2010 and 2012-2013. *Journal of Atmospheric and Solar-Terrestrial Physics*, *154*, 132–166. Retrieved from https://www.sciencedirect.com/science/article/pii/S1364682616303182

Merzlyakov, E. G., Solovyova, T. V., & Yudakov, A. A. (2012). Interannual variability of the spring transition date in the MLT region observed with meteor radar at Obninsk (55°N, 37°E). *Journal of Atmospheric and Solar-Terrestrial Physics*, *77*, 113–118. https://doi.org/10.1016/j.jastp.2011.12.006

Mitchell, N. J., Pancheva, D., Middleton, H. R., & Hagan, M. E. (2002). Mean winds and tides in the arctic mesosphere and lower thermosphere. *Journal of Geophysical Research*, *107*(A1), SIA21214. https://doi.org/10.1029/2001ja900127

Molod, A., Takacs, L., Suarez, M., & Bacmeister, J. (2015). Development of the GEOS-5 atmospheric general circulation model: Evolution from MERRA to MERRA2. *Geoscientific Model Development*, *8*(5), 1339–1356. https://doi.org/10.5194/gmd-8-1339-2015

Nash, E. R., Newman, P. A., Rosenfield, J. E., & Schoeberl, M. R. (1996). An objective determination of the polar vortex using Ertel's potential vorticity. *Journal of Geophysical Research*, *101*(D5), 9471–9478. https://doi.org/10.1029/96JD00066

Newman, P. A., Nash, E. R., & Rosenfield, J. E. (2001). What controls the temperature of the Arctic stratosphere during the spring? *Journal of Geophysical Research*, *106*(D17), 19999–20010. https://doi.org/10.1029/2000JD000061

Salby, M. L., & Callaghan, P. F. (2007). Influence of planetary wave activity on the stratospheric final warming and spring ozone. *Journal of Geophysical Research*, *112*(D20). https://doi.org/10.1029/2006JD007536

Savenkova, E. N., Kanukhina, A. Y., Pogoreltsev, A. I., & Merzlyakov, E. G. (2012). Variability of the springtime transition date and planetary waves in the stratosphere. *Journal of Atmospheric and Solar-Terrestrial Physics*, *90–91*, 1–8. https://doi.org/10.1016/j.jastp.2011.11.001

Shepherd, G. G., Stegman, J., Espy, P., McLandress, C., Thuillier, G., & Wiens, R. H. (1999). Springtime transition in lower thermospheric atomic oxygen. *Journal of Geophysical Research*, *104*(A1), 213–223. https://doi.org/10.1029/98JA02831

Shepherd, M. G., Espy, P. J., She, C. Y., Hocking, W., Keckhut, P., Gavrilyeva, G., et al. (2002). Springtime transition in upper mesospheric temperature in the northern hemisphere. *Journal of Atmospheric and Solar-Terrestrial Physics*, *64*(8), 1183–1199. https://doi.org/10.1016/S1364-6826(02)00068-8

Stober, G., Baumgarten, K., McCormack, J. P., Brown, P., & Czarnecki, J. (2020). Comparative study between ground-based observations and NAVGEM-HA analysis data in the mesosphere and lower thermosphere region. *Atmospheric Chemistry and Physics*, *20*(20), 11979–12010. https://doi.org/10.5194/acp-20-11979-2020

Thiélemont, R., Ayarzagüena, B., Matthes, K., Bekki, S., Abalichin, J., & Langematz, U. (2019). Drivers and surface signal of interannual variability of boreal stratospheric final warmings. *Journal of Geophysical Research: Atmospheres*, *124*(10), 5400–5417. https://doi.org/10.1029/2018JD029852

Wang, T., Zhang, Q., Hannachi, A., Lin, Y., & Hirooka, T. (2019). On the dynamics of the spring seasonal transition in the two hemispheric high-latitude stratosphere. *Tellus A: Dynamic Meteorology and Oceanography*, *71*(1), 1634949. https://doi.org/10.1080/16000870.2019.1634949

Waters, J. W., Froidevaux, L., Harwood, R. S., Jarnot, R. F., Pickett, H. M., Read, W. G., et al. (2006). The earth observing system microwave limb sounder (EOS MLS) on the aura satellite. *IEEE Transactions on Geoscience and Remote Sensing*, *44*(5), 1075–1092. https://doi.org/10.1109/TGRS.2006.873771

Waugh, D. W., Randel, W. J., Pawson, S., Newman, P. A., & Nash, E. R. (1999). Persistence of the lower stratospheric polar vortices. *Journal of Geophysical Research*, *104*(D22), 27191–27201. https://doi.org/10.1029/1999JD900795

Waugh, D. W., & Rong, P.-P. (2002). Interannual variability in the decay of lower stratospheric Arctic vortices. *Journal of the Meteorological Society of Japan*, *80*(4B), 997–1012. https://doi.org/10.2151/jmsj.80.997

Wei, K., Chen, W., & Huang, R. (2007). Dynamical diagnosis of the breakup of the stratospheric polar vortex in the Northern Hemisphere. *Science in China, Series D*, *50*(9), 1369–1379. https://doi.org/10.1007/s11430-007-0100-2

Yamazaki, Y., & Matthias, V. (2019). Large-amplitude quasi-10-day waves in the middle atmosphere during final warmings. *Journal of Geophysical Research: Atmospheres*, *124*(17–18), 9874–9892. https://doi.org/10.1029/2019JD030634

Yiğit, E., & Medvedev, A. S. (2015). Internal wave coupling processes in Earth's atmosphere. *Advances in Space Research*, *55*(4), 983–1003. https://doi.org/10.1016/j.asr.2014.11.020

Yu, F. R., Huang, K. M., Zhang, S. D., Huang, C. M., Yi, F., Gong, Y., et al. (2019). Quasi 10- and 16-day wave activities observed through meteor radar and MST radar during stratospheric final warming in 2015 spring. *Journal of Geophysical Research: Atmospheres*, *124*(12), 6040–6056. https://doi.org/10.1029/2019JD030630